Nanocomposites—a new material design concept

ELSEVIER

Science and Technology of Advanced Materials 6 (2005) 2–10

SCIENCE AND TECHNOLOGY OF ADVANCED MATERIALS

www.elsevier.com/locate/stam

Nanocomposites—a new material design concept

Seong-Min Choi, Hideo Awaji*

Department of Environmental and Materials Engineering, Nagoya Institute of Technology, Gokiso-cho, Showa-ku, Nagoya 466-8555, Japan

Received 30 March 2004; revised 29 June 2004; accepted 15 July 2004
Available online 15 December 2004

Abstract

Ceramic-based nanocomposites were reviewed, emphasizing the newly developed concept of material design for ceramics. First, characteristics of the nanocomposites observed by previous researchers were summarized as, significant or moderate improvement in strength, drastic change of the fracture mode from intergranular fracture of monolithic ceramics to transgranular fracture of nanocomposites, moderate enhancement of fracture toughness, improvement of other mechanical properties, and observations of dislocations. Second, several mechanisms proposed previously to explain these characteristics were reviewed. Third, our strengthening and toughening mechanisms of nanocomposites on the basis of dislocation activities were explained. In nanocomposites, the highly localized residual stresses in the matrix grains are generated by the mismatch of thermal expansion coefficients between the matrix and the dispersed particles, and the dislocations are yielded during the cooling process after sintering. These dislocations then release the tensile residual stresses intrinsically existing in the matrix grains of sintered ceramics and improve the strength of the materials. In addition, as these dislocations cannot move at room temperature the sessile dislocations in the matrix operate as nano-crack nuclei in a frontal process zone (FPZ) ahead of the crack tip when the tip of a propagating crack approaches this area. Therefore, the size of the FPZ is expanded and as a result the fracture toughness is improved. Finally, estimation of the critical FPZ size was explained in order to clarify its toughening mechanism in nanocomposites.

Keywords: Nanocomposites; Ceramics; Dislocation; Strengthening mechanism; Toughening mechanism; Frontal process zone

Contents

* Corresponding author. Tel./fax: +81 52 735 5276.
E-mail address: awaji@nitech.ac.jp (H. Awaji).

1468-6996/$ - see front matter © 2004 Elsevier Ltd. All rights reserved.
doi:10.1016/j.stam.2004.07.001

1. Introduction

Structural ceramics exhibit several excellent properties, such as high thermal resistance, good chemical stability, and mechanical strength. However, ceramics have a low fracture toughness because of their ionic and covalent bonds, hence the plastic deformation of structural ceramics due to dislocation movement is extremely limited. To overcome the inherent brittleness of ceramics, a new material design concept must be developed [1].

During the past two decades, much effort has been directed toward improving the fracture toughness of ceramics mainly from the view point of redistributing stress at the crack tip [2,3]. The techniques are crack-surface bridging [4], particle dispersion of different phases in a matrix [5], fiber-reinforced composites [2], macroscopic crack deflection [6,7], and phase transformation/microcracking in zirconia [8,9]. Among them, macroscopic crack deflection in multi-layered ceramic composites and continuous fiber-reinforced ceramic-based composites are based on different design concepts from the others. In this review, we will focus our attention on ceramic-matrix materials with macroscopically homogeneous structures.

Several techniques for improving the fracture toughness of ceramics have been proposed by many researchers. Whiskers or short fibers were used for reinforcing ceramics, while column-like grains reinforce silicon nitride and alumina by themselves. Second-phase particles dispersed within the matrix were used to improve fracture toughness of ceramics. However, the effects of these second-phase whiskers, short fibers, and particles were limited [5].

Nanocomposites proposed by Niihara [1] have a new material design concept and significantly improved strength has been achieved with moderate enhancement in fracture toughness. The microstructure of nanocomposites is constructed by dispersing second-phase nano-size particles within the matrix grains and on the grain boundaries. Thermal expansion mismatch between the matrix and second-phase particles produces a marked improvement in mechanical properties such as fracture strength, fracture toughness, creep resistance, thermal shock resistance, and wear resistance.

Even though several models for the mechanisms of nanocomposites have been proposed [10,11], such as a steep *R*-curve behavior model [12], residual stress model [13], and reduction in the processing defect size model [14], several researchers remain skeptical about nanocomposites [15,16]. These skepticisms result from the fact that the previously proposed strengthening and toughening mechanisms mentioned above do not provide sufficient explanations for all of the characteristics of nanocomposites that have been observed.

The aim of this review is to summarize the characteristics of nanocomposites observed by several researchers, to give our explanations for the strengthening and toughening mechanisms of nanocomposites associated with dislocation activities, even in brittle ceramics, and to discuss the role of the frontal process zone (FPZ) size ahead of a crack tip in nanocomposites. We have restricted our attention to the alumina-based nanocomposites in order to simplify the following discussions.

2. Characteristics of nanocomposites

Basic microstructures in nanocomposites are classified into three types: intra-type, inter-type, and nano/nano-type [1]. With respect to mechanical properties such as strength and fracture toughness, the most important structure is an intra-type nanostructure where dispersed particles are embedded within the matrix grains, as shown in Fig. 1. The highest strength or fracture toughness is mostly achieved when only a few percent of the second-phase particles are dispersed in alumina. According to observations regarding alumina/silicon carbide system by transmission electron microscopy (TEM), silicon carbide nano-size particles are dispersed homogeneously both inside the alumina grains and on the grain boundaries [1,17]. Moreover, there are advantages such as that ceramics with a low percent of second-phase particles have better sinterability, while less dispersed particles have a higher possibility of existing in matrix grains. The intra-type microstructure of alumina/silicon carbide nanocomposites observed by our group [17] is shown in Fig. 2.

The characteristics of nanocomposites observed by many researchers are summarized as follows; (A) drastic change of fracture mode from intergranular fracture of monolithic alumina to transgranular fracture of nanocomposites, (B) moderate to significant improvement in strength, (C) moderate improvement of fracture toughness, and (D) improvement of several mechanical properties. The transgranular fracture mode in nanocomposites is a typical

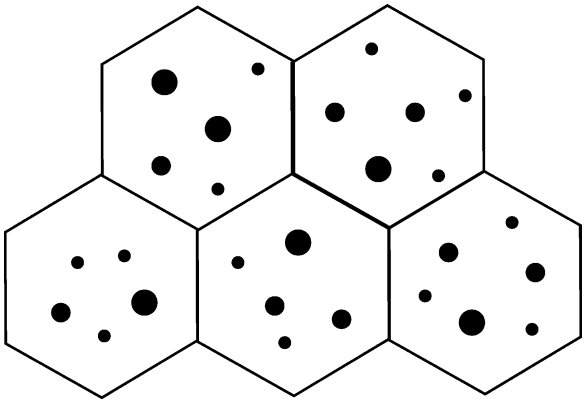

Fig. 1. Intra-type nanostructure.

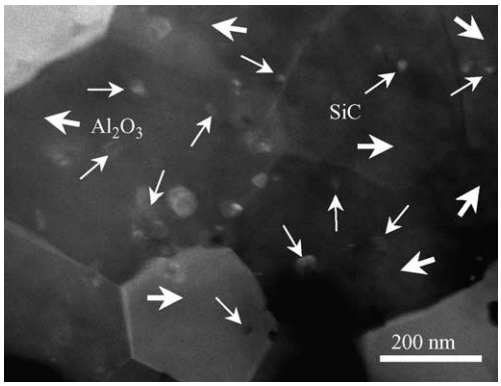

Fig. 2. TEM observation of alumina grains within nano-sized silicon carbide (SiC) particles.

and easily observed characteristic. Fig. 3 compares the difference of the fracture surface between the monolithic alumina and the alumina/cupper nanocomposites [18]. Although monolithic alumina indicates an intergranular fracture mode, only a few volume percent of the second-phase particles changes the fracture mode drastically from intergranular fracture to transgranular fracture.

Several researchers have reported a moderate enhancement of fracture toughness with improved strength in nanocomposites, for instance, Niihara [1], Davidge et al. [11], Carroll et al. [14], Zhao et al. [19], and Gao et al. [20], in spite of the well-known trade-off relations between the strength and the fracture toughness of monolithic ceramics [8]. Several mechanical properties were also improved, such as hardness [14,20,21], wear resistance [1,5], thermal shock resistance [1], and creep resistance [1,5]. On the other hand, Niihara observed highly developed sub-grain boundaries or dislocation networks in annealed nanocomposites [1], and several researchers have observed embryonic dislocations in the matrix grains [22]. Fig. 4 shows dislocations in alumina/silicon carbide nanocomposites [23]. Strengthening and toughening mechanisms of nanocomposites must explain these characteristics without any inconsistencies.

3. Mechanisms of nanocomposites

3.1. Previous models

The previously proposed strengthening and toughening mechanisms of nanocomposites are reviewed first. Sternitzke [10] reviewed the modeling (strengthening and toughening mechanisms) of nanocomposites and divided the mechanisms into three groups; c-mechanism where the critical flaw size is reduced, K-mechanism where the fracture toughness is increased, and grain boundary strengthening mechanism. The c-mechanism is based on the fact that the matrix becomes refined following the adding of nano-sized silicon carbide. A refinement of the grain size leads to smaller critical flaw size and higher strength following the Hall–Petch relation.

K-mechanism relates to *R*-curve behavior, crack deflection, and crack bowing during a crack extension. Ohji et al. [12] proposed a particle-bridge mechanism, whereby crack-face shielding results when nano-size particles bridge the crack surfaces. Crack deflection and crack bowing are related to the interactions of a crack front with second-phase inclusions which depend on the differences in the thermo-elastic properties of the matrix and inclusions. Many researchers have studied this mechanism previously as a particle reinforced toughening mechanism and it is known that the particles do not have sufficient effects in the case that the dispersed particles are not nano-sized. Levin et al. [13] and Sekino et al. [24] explained that the strengthening mechanism of nanocomposites results from residual stresses around the second-phase particles using the Selsing equation [25], and matrix weakening and grain boundary strengthening produce the change of the fracture mode. Only nano-sized dispersed particles can improve the strength and the fracture toughness. These mechanisms will be explained in the next section.

Much observation indicates that matrix grain boundaries are strengthened in nanocomposites. Levin et al. [13] have presented a model showing the influence of silicon carbide particles on the fracture toughness of nanocomposites. Silicon carbide particles within the matrix grains

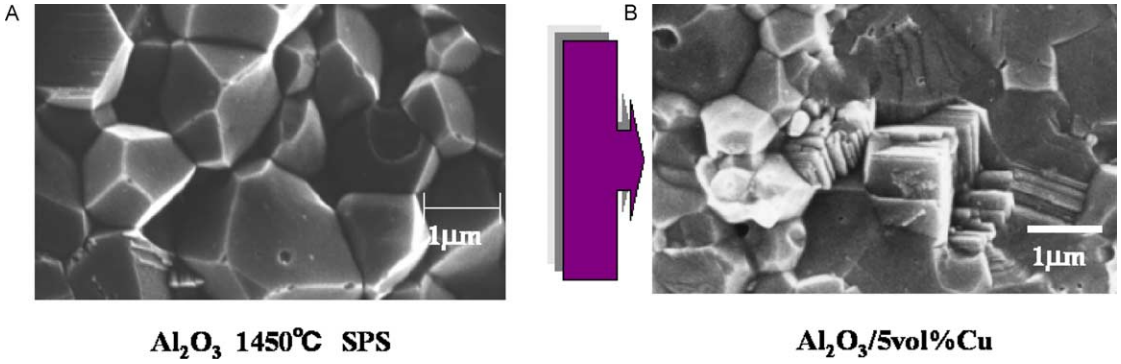

Fig. 3. Fracture surfaces of monolithic alumina (A) and nanocomposites (B).

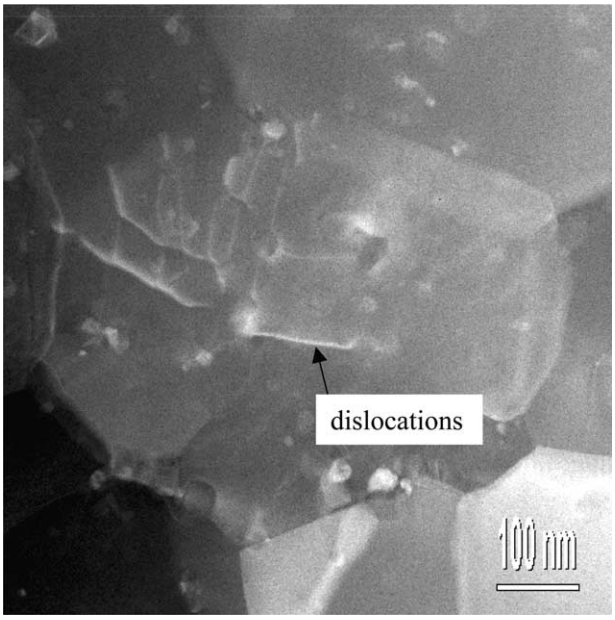

Fig. 4. TEM observation of dislocations in alumina/silicon carbide nanocomposites.

strengthen the grain boundaries because of compressive radial stresses, where the matrix (alumina) has a larger thermal expansion coefficient than the particle (silicon carbide). However, tensile residual stresses also improve the strength and fracture toughness, for example; the silicon nitride/silicon carbide system. Some researchers say that improvement of the strength of nanocomposites is based on the surface residual stresses following machining [15], however, the residual stresses caused by machining are limited. None of these mechanisms can explain all of the characteristics mentioned above.

3.2. Dislocation model

Nanocomposites consist of nano-particles dispersed within matrix grains. The microstructural characteristic of these nanocomposites results in the generation of thermally induced residual stresses after sintering. To clarify the role of the residual stresses around the dispersed particles in nanocomposites, Awaji et al. [26] analyzed residual stresses using a simplified model that consisted of a spherical particle within a concentric matrix sphere with axial symmetry, shown in Fig. 5.

Residual stresses numerically calculated on the particle-matrix boundary for alumina/silicon carbide nanocomposites are shown in Table 1, where we assumed that the temperature difference was 1570 °C and that the ratio of the particle/matrix radii was 1/5. In Table 1, the symbols with suffix p indicate the properties of the particle (silicon carbide) and the symbols with suffix m are the properties of the matrix (alumina). It is noted that there is a large maximum shear stress on the boundary.

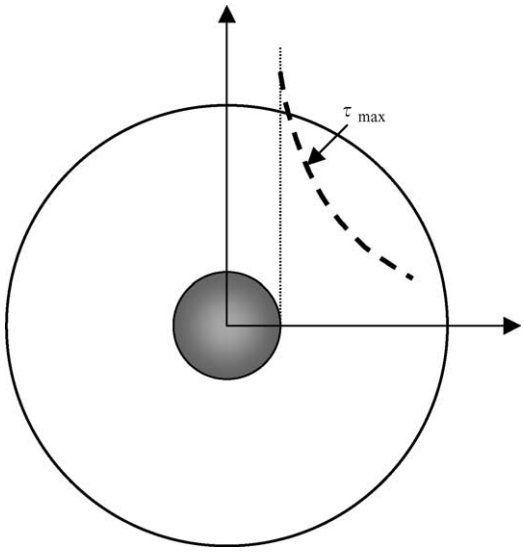

Fig. 5. A model of intra-type nanostructure.

Lagerlöf et al. [27] reported that the temperature dependence of both basal and prism plane slips in a single α-alumina crystal could be described by a simple logarithmic law over a wide range of temperatures:

$$\ln \tau_{cb} = \ln \tau_0 - 0.0052T, \quad (1)$$

and

$$\ln \tau_{cp} = \ln \tau_0 - 0.0026T, \quad (2)$$

where τ_{cb} and τ_{cp} indicate the critical resolved shear stresses for basal and prism plane slips, respectively, T is temperature [K], and $\tau_0 = 109$ and 9 GPa for basal and prism plane slips, respectively. Fig. 6 shows the temperature dependencies of the critical resolved shear stresses for basal and prism plane slips in a single α-alumina crystal and the residual shear stress on the alumina/silicon carbide boundary in nanocomposites, where τ_{res} is the maximum residual shear stress on the boundary of alumina/silicon carbide, based on the assumption that the residual stress is linearly related to temperature. This figure indicates that dislocation movements are possible in the alumina grains at temperatures ranging from 600 to 1400 °C, suggesting that this temperature range is quite important in creating dislocations in the alumina matrix during the cooling process following nanocomposites sintering or the annealing process. Therefore, control of the cooling rate and pressure during the cooling process is required for the creation of dislocations. Further, annealing will lead to the

Table 1
Residual stresses along the particle-matrix boundary in alumina/silicon carbide nanocomposites under the assumption of $\Delta T = 1570$ °C and the ratio of the particle and matrix radii is 1/5

System	$\alpha_m/\alpha_p \times 10^{-6}$ (K^{-1})	E_m/E_p (GPa)	ν_m/ν_p	σ_θ (GPa)	T_{max} (GPa)
Al_2O_3/Sic	8.8/4.7	380/490	0.21/0.19	1.16	1.71

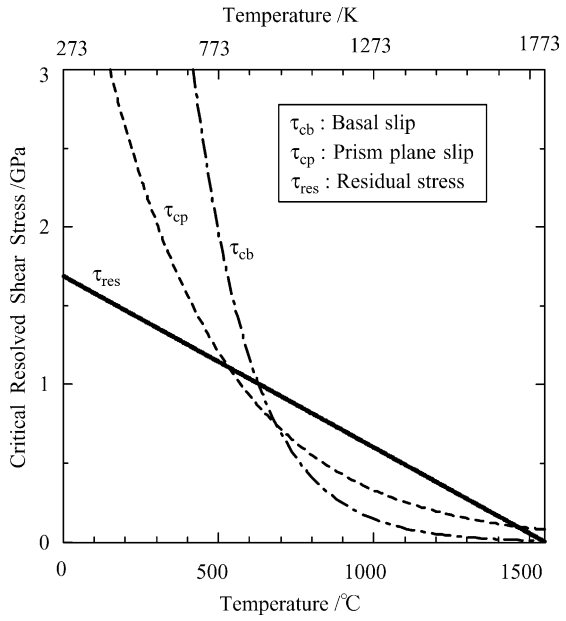

Fig. 6. Temperature dependencies of the critical resolved shear stresses in α-alumina and the residual shear stress in the boundary of alumina–silicon carbide in nanocomposites.

development of sub-grain boundaries as a result of dislocation rearrangement.

The mismatches in thermal expansion and Young's modulus between the matrix and the dispersed particles yield highly localized residual stresses around the particles. These stresses reduce quickly as distance from the boundary increases because of the nano-sized particles, which can generate only small defects such as dislocations in close vicinity to the particles, as shown in Fig. 7(A). Large-scale cracks or other large defects will be difficult to create in the nanocompsoite system, while only dislocations can disperse in matrix grains at high temperatures. These dislocations are considered to become nano-crack nuclei at room temperature because the critical resolved shear stresses at room temperature for prism plane slip and basal slip are estimated to be 4.2 and 23.1 GPa, respectively, from Eq. (2), which are higher than the theoretical strength, 2.6 GPa, of the α-alumina. This fact suggests that further annealing following sintering is important in dispersing dislocations into the matrix grain, as shown in Fig. 7(B).

3.3. Toughening mechanism

Crack extension resistance in polycrystalline ceramics with *R*-curve behavior is expressed as [28]

$$K_R(\Delta a) = K_i + \Delta K_R(\Delta a) \quad (3)$$

where $K_R(\Delta a)$ represents the fracture toughness of the material exhibiting *R*-curve behavior, K_i is the intrinsic fracture toughness, and $\Delta K_R(\Delta a)$ is the extrinsic increase in the fracture toughness after a certain extension from the initial crack tip, Δa.

A schematic diagram explaining crack extension resistances in polycrystalline ceramics with rising *R*-curve behavior is shown in Fig. 8 [29]. Comparison of Eq. (3) and Fig. 8 indicates that the intrinsic fracture toughness, K_i, is related to the energy required to create the damaged FPZ at the crack tip, and that ΔK_R is caused by the shielding effects of bridging in a process zone wake. Thus, there are two mechanisms for improving the fracture toughness in polycrystalline ceramics. One mechanism is the process zone toughening mechanism which creates a damaged zone in front of a crack tip. Therefore, to improve the intrinsic fracture toughness, the fracture energy consumed in the process zone must be increased. The other mechanism is the crack-surface bridging toughening mechanism operating in a process zone wake which produces an extrinsic increase in crack resistance after a certain extension of the crack from the initial crack length. The toughening mechanism in nanocomposites is mainly the process zone toughening mechanism [26].

Fig. 9 shows a schematic illustration of the toughening mechanism of nanocomposites [26]. Dispersed dislocations within the matrix grains after annealing for alumina/silicon carbide nanocomposites are described in this figure. In a matrix grain, sub-grain boundaries or dislocation networks are generated around the nano-sized silicon carbide particles and the sessile dislocations are

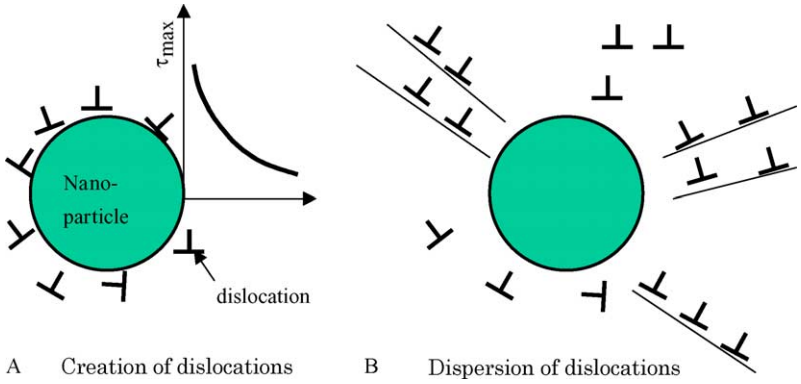

Fig. 7. Dislocations after sintering (A) and after annealing (B).

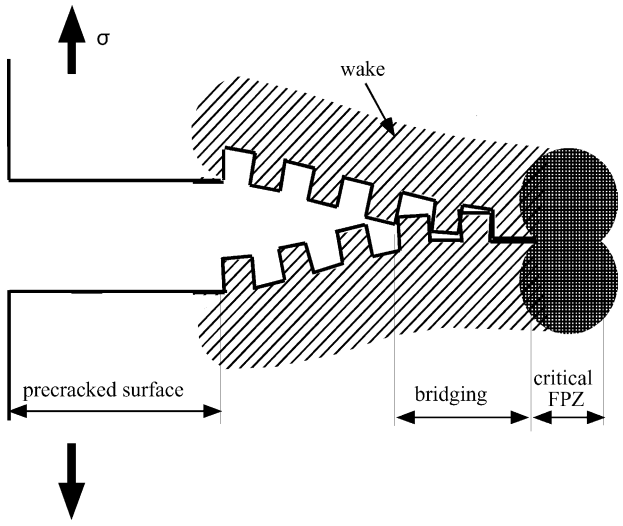

Fig. 8. Schematic diagram of a frontal process zone and bridging in polycrystalline ceramics with *R*-curve behavior.

dispersed in the matrix, shown in Fig. 9(A). In this situation, when the tip of a propagating large crack reaches this area, these sessile dislocations in the matrix will operate as nano-crack nuclei in the vicinity of the propagating crack tip, shown in Fig. 9(B). The highly stressed state in the FPZ is then released by nano-crack nucleation, and the nano-cracks expand the FPZ size, enhancing the intrinsic fracture toughness of the materials.

3.4. Strengthening mechanism

The grains and grain boundaries of sintered alumina contain tensile residual stresses resulting from anisotropic thermal expansion, Young's modulus along the crystal axes, and crystallographic misorientation across the grain boundaries. Therefore, in the sintered polycrystalline alumina, it is conceivable that the large crack along a grain boundary created by the synergetic effects of both residual stresses and processing defects, will be equivalent to the grain size of the material and that the weakest crack generated along a boundary in the specimen will dominate the strength of the specimen. The fracture toughness of grain boundaries is usually lower than that within the grains. Hence, polycrystalline alumina ceramics exhibit a mainly intergranular fracture mode, as schematically shown in Fig. 10(A). Fig. 3(A) also shows the scanning electron microscopy (SEM) observation of the fracture surface of monolithic alumina.

Nanocomposites, however, will yield dislocations around the particles, and the dislocations release residual stresses in the matrix. Consequently, the defect size along the grain boundaries is reduced in nanocompsoites, as shown in Fig. 10(B). Also, the dislocations are difficult to move in ceramics at room temperature, serve as origins of small stress concentrations, and create nano-cracks around the propagating crack tip. These nano-cracks slightly reduce the strength of the alumina matrix, while reduction of both the residual stresses along the grain boundaries and the strength in the matrix are attributable to a change in the fracture mode from that of the intergranular fracture in monolithic alumina to that of the transgranular fracture in nanocomposites. Also, the fracture surface of the transgranular mode of nanocomposites is not a simple planar cleavage plane. Several steps are frequently observed on the surface and are likely to be evidence of nano-cracking in the FPZ wake. Fig. 3(B) shows an SEM micrograph of a fracture surface of alumina/5 vol% copper nanocomposites [18], where step-wise fracture surface is observed.

Reduction of both the defect size along the grain boundaries and the tensile residual stresses in the matrix grains by dislocations result in improvement of the strength of nanocomposites. Several mechanical properties of nanocomposites are also improved for the same reason, such as hardness, wear resistance, creep resistance,

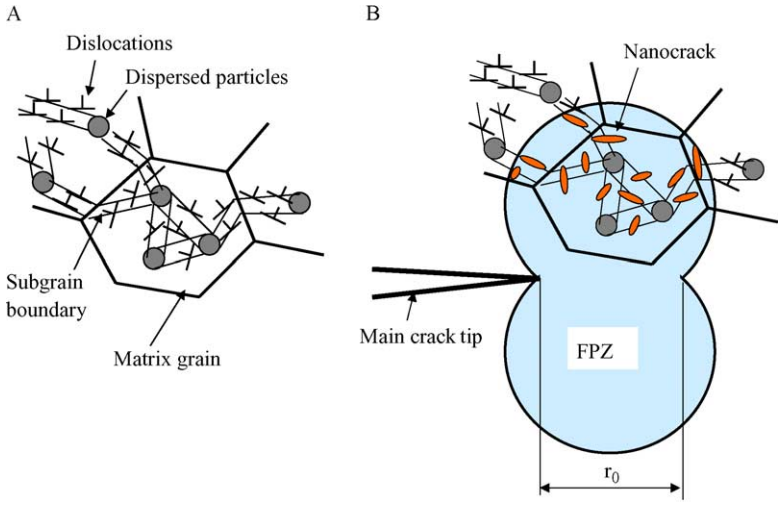

Fig. 9. Schematic description of the toughening mechanism in nanocomposites. (A) Intra-type nano-structure after annealing, (B) FPZ creation.

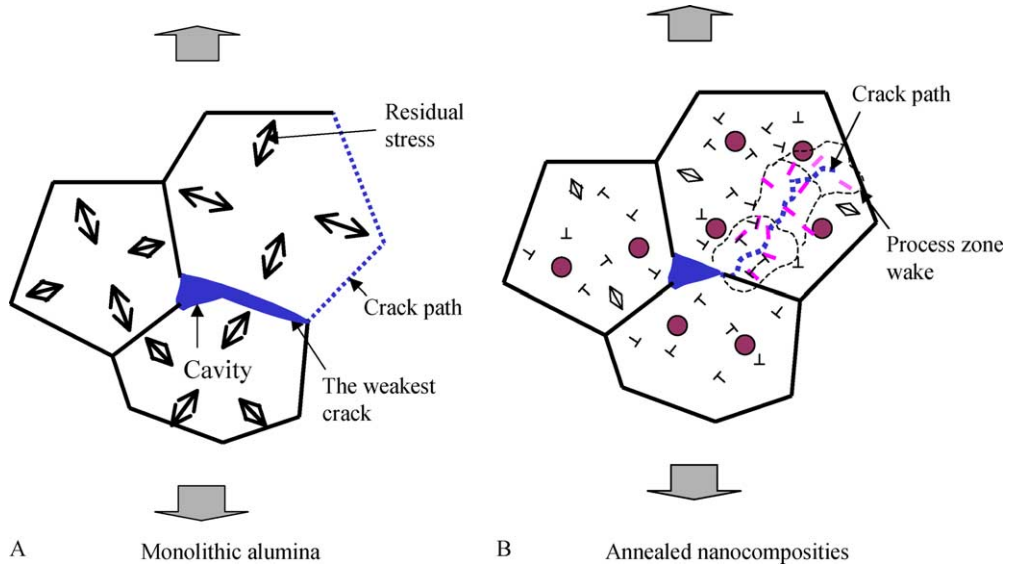

Fig. 10. Schematic diagram of the strengthening mechanism in nanocomposites.

and thermal shock resistance. Davidge et al. [5] reported drastic changes in the abrasive wear surfaces between monolithic alumina and nanocomposites, where the surface of monolithic alumina showed grain pullout. The nanocomposites, however, showed ground or abraded surfaces because of the improved strength along the grain boundaries.

3.5. Frontal process zone size

Ceramics have low fracture toughness because of their ionic and covalent bonds hence, the plastic deformation in structural ceramics due to dislocation movement is extremely limited, particularly at room temperature. Therefore, the FPZ ahead of a crack tip is considered to be composed of many micro-cracks or nano-cracks rather than dislocations as in metals [30,31]. Although the critical size of the FPZ is considered to be an important factor for assessing toughening mechanisms, there is no direct means of measuring the critical size of the FPZ.

Recently, we proposed a novel technique for estimating the critical size of the FPZ in ceramics [32–34] using a single-edge V-notched beam (SEVNB) method [35,36] on the basis of the local fracture criterion. The local fracture criterion states that a crack will propagate when the stress at the characteristic distance from the crack tip reaches the critical value [37]. Fig. 11 shows the stress distribution on the r-axis ahead of a crack tip when the crack length is long enough compared to the critical FPZ size, r_0, that is to say, linear fracture mechanics is applicable in this case. The stress intensity approximation can be adopted for the stress at r_0. If the characteristic distance is equal to the critical frontal process zone size, as shown in Fig. 11, the following relation is derived,

$$\sigma_c = \frac{K_{IC}}{\sqrt{2\pi r_0}}, \tag{4}$$

where σ_c represents the local fracture stress defined at r_0. The critical FPZ size is then derived [38]

$$r_0 = \frac{1}{2\pi}\left(\frac{K_{IC}}{\sigma_c}\right)^2. \tag{5}$$

The exact stress distribution, σ_y, along r-axis in an infinite plate under a critical stress state is expressed as

$$\sigma_y = \frac{\sigma_{fc}(a_e + r)}{\sqrt{2a_e r + r^2}}, \tag{6}$$

where σ_{fc} represents the critical remote stress and a_e is the half crack length in an infinite plate. Therefore, the relation between the local fracture stress, σ_c, at r_0 and

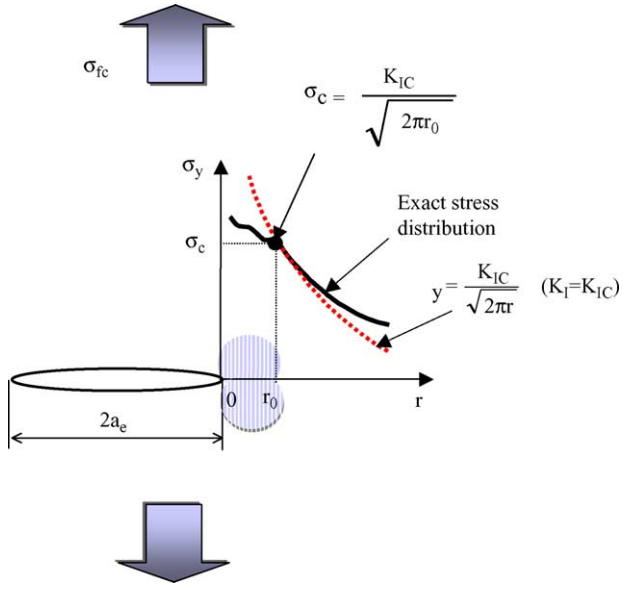

Fig. 11. Exact stress distribution and its stress intensity factor approximation at a crack tip in an infinite plate under a critical stress state.

the critical remote stress, σ_{fc}, is derived as

$$\sigma_{fc} = \sigma_c \frac{\sqrt{2a_e r_0 + r_0^2}}{a_e + r_0} \quad (7)$$

If we let $a_e \to 0$, the following relation is derived

$$\lim_{a_e \to 0} \sigma_{fc} \to \sigma_c \quad (8)$$

The value of σ_c is, therefore, considered to be the strength of the infinite plate with no artificial crack. However, actual materials have inherent cracks and the weakest crack dominates the strength. The difference between the strength of actual materials and the value of σ_c is then considered to be the difference between their effective volumes, where the effective volume is the critical FPZ size.

Fig. 12 shows the relation between the flexural strength and the local fracture stress for monolithic alumina, where the double circles indicates the flexural strength of notched specimens, σ_B is the flexural strength with no artificial notch, σ_c is the estimated local fracture stress calculated from their effective volumes, and the dot-dashed line indicates Eq. (7).

Table 2 shows the experimental results for monolithic alumina and alumina-based nanocomposites. In this table, Al_2O_3 is monolithic alumina of 99.5% purity with a minor dopant of MgO with a mean grain size of 2 μm (manufactured by Japan Fine Ceramics Center), Al_2O_3/5 wt% Ni and Al_2O_3/3 vol% SiC are nanocomposites fabricated by us [23,39], the value r_0 is calculated from Eq. (5), and r_0^* is the approximated value calculated from the following equation using the σ_B instead of the σ_c

$$r_0^* \approx \frac{1}{2\pi}\left(\frac{K_{IC}}{\sigma_c}\right)^2. \quad (9)$$

On comparing these data in the table, it is clear that the fracture strengths of nanocomposites are higher than alumina, and the fracture toughness of nanocompsites are also higher than that of alumina. However, the critical FPZ sizes of the nanocomposites are not always higher than that of alumina.

Table 2
Experimental results for alumina and alumina-based nanocomposites

Specimens	Fracture strength σ_B (Mpa)	Fracture toughness K_{IC} (MPa $m^{1/2}$)	Critical FPZ size r_0^* (r_0) (μm)	$\sigma_B r_0^{1/2}$ (MPa $m^{1/2}$)
Al_2O_3	462	3.72	10.3 (6.9)	1.21
Al_2O_3/ 5 wt%Ni	462	4.00	11.9 (9.0)	1.39
Al_2O_3/ 3 vol%SiC	760	5.06	7.1 (5.3)	1.75

Fig. 13 shows the relation between the fracture toughness and the product of the σ_B and $r_0^{1/2}$ for monolithic alumina and alumina-based nanocomposites. It notes that the values of the fracture toughness of the nanocomposites are higher than that of the monolithic alumina, and that improvement of the fracture toughness of ceramics requires greater values of both the strength and the critical FPZ size.

4. Conclusions

Alumina-based nanocomposites were reviewed on the basis of previous reports and our calculated and experimentally obtained results, emphasizing its newly developed concept of material design for ceramics. Toughening and strengthening mechanisms of alumina-based nanocomposites were discussed in association with dislocation activities in alumina. The critical size of the frontal process zone for nanocomposites was estimated on the basis of the local fracture criterion and we clarified that to improve the fracture toughness, both the strength and the critical frontal process zone size of materials must be increased.

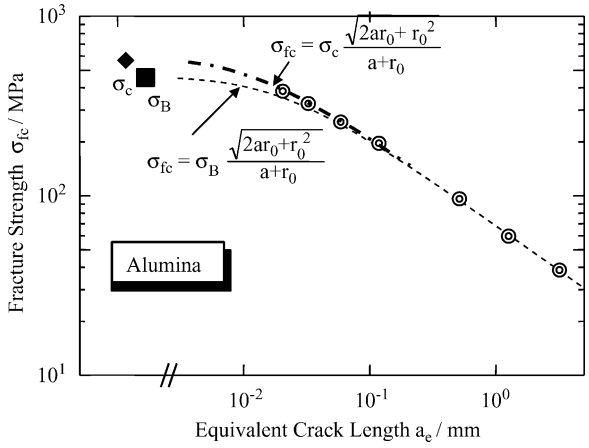

Fig. 12. Experimentally obtained the flexural strengths of notched specimen ◎, the flexure strength of unnotched specimen, σ_B, and the local fracture stress, σ_c.

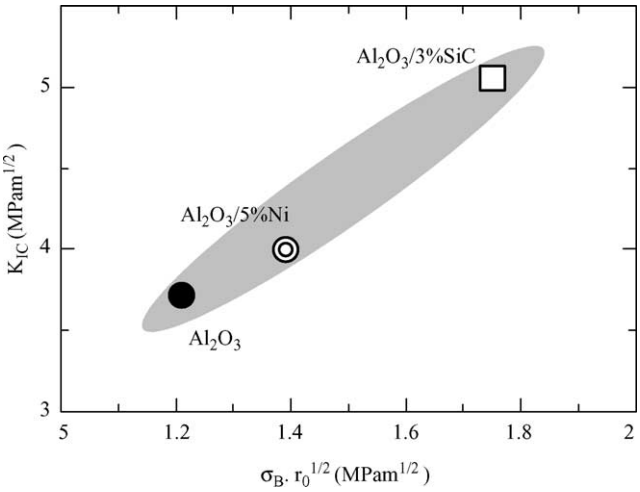

Fig. 13. Relation between the fracture strength and $\sigma_B\, r_0^{1/2}$.

Acknowledgements

We received a grant from the NITECH 21st Century COE Program 'World Ceramics Center for Environmental Harmony'.

References

[1] K. Niihara, New design concept of structural ceramics—ceramic nanocomposites, J. Ceram. Soc. Japan 99 (1991) 974–982.
[2] A.G. Evans, Perspective on the development of high-toughness ceramics, J. Am. Ceram. Soc. 73 (1990) 187–206.
[3] S. Dutta, Fracture toughness and reliability in high-temperature structural ceramics and composites: prospects and challenges for the 21st century, Bull. Mater. Sci. 24 (2001) 117–120.
[4] D.J. Green, An Introduction to the Mechanical Properties of Ceramics, Cambridge University Press, 1998.
[5] R.W. Davidge, in: R.C. Bradt, D.P.H. Hasselman, F.F. Lange (Eds.), Effect of microstructure on the mechanical properties of ceramics, Fracture Mechanics of Ceramics vol. 2, Plenum Press, New York, 1973, pp. 447–468.
[6] W.J. Clegg, K. Kendall, N.McN. Alford, T.W. Button, J.D. Birchall, A simple way to make tough ceramics, Nature 347 (1990) 455–457.
[7] H. Awaji, M. Ebisudani, S-M. Choi, Crack deflection toughening mechanism in brittle materials in: J.A. Salem, G.D. Quinn, M.G. Jenkins (Eds.), ASTM STP 1409 (2002), pp. 137–151.
[8] M.V. Swain, Inelastic deformation of Mg-PSZ and its significance for strength–toughness relationship of zirconia toughened ceramics, Acta Metall. 33 (1985) 2083–2091.
[9] M. Rühle, N. Claussen, A.H. Heuer, Transformation and microcrack toughening as complementary processes in ZrO_2-toughened Al_2O_3, J. Am. Ceram. Soc. 69 (1986) 195–197.
[10] M. Sternitzke, Review: structural ceramic nanocomposites, J. Eur. Ceram. Soc. 17 (1997) 1061–1082.
[11] R.W. Davidge, R.J. Brook, F. Cambier, M. Poorteman, A. Leriche, D. O'Sullivan, S. Hampshire, T. Kennedy, Fabrication, properties, and modeling of engineering ceramics reinforced with nanoparticles of silicon carbide, Br. Ceram. Trans. 96 (1997) 121–127.
[12] T. Ohji, Y-K. Jeong, Y-H. Choa, K. Niihara, Strengthening and toughening mechanisms of ceramic nanocomposites, J. Am. Ceram. Soc. 81 (1998) 1453–1460.
[13] I. Levin, W.D. Kaplan, D.G. Brandon, A. Layous, J. Am. Ceram. Soc. 78 (1995) 254–256.
[14] L. Carroll, M. Sternitzke, B. Derby, Silicon carbide particle size effects in alumina-based nanocomposites, Acta Mater. 44 (1996) 4543–4552.
[15] G. Pezzotti, V. Sergo, K. Ota, O. Sbaizero, N. Murai, T. Nishida, M. Sakai, Residual stresses and apparent strengthening in ceramic-matrix nanocomposites, J. Ceram. Soc. Jpn 104 (1996) 497–503.
[16] J. Pérez-Rigueiro, J.Y. Pastor, J. Llorca, M. Elices, P. Miranzo, S. Moya, Revisiting the mechanical behavior of alumina/silicon carbide nanocomposites, Acta Mater. 46 (1998) 5399–5411.
[17] H. Awaji, S-M. Choi, Review: ceramic-based nanocomposites in: S.G. Pandalai (Ed.), Recent Research Developments in Materials Science & Engineering vol. 1 2002, pp. 585–597.
[18] S.-M. Choi, S. Honda, T. Nishikawa, H. Awaji, F.D. Gnanam, K. vishista, T. Kuroyama, Design concept of strengthening and toughening mechanisms in nanocomposites—ceramic metal nanocomposites, J. Ceram. Soc. Jpn. 112 (2004) S912–S915.
[19] J. Zhao, L.C. Steans, M.P. Harmer, H.M. Chan, G.A. Miller, R.F. Cook, Mechanical behavior of alumina–silicon carbide nanocomposites, J. Am. Ceram. Soc. 76 (1993) 503–510.
[20] L. Gao, H.Z. Wang, J.S. Hong, H. Miyamoto, K. Miyamoto, Y. Nishikawa, D. de la Torre, Mechanical properties and microstructures of nano-SiC–Al_2O_3 composites densified by spark plasma sintering, J. Eur. Ceram. Soc. 19 (1999) 609–613.
[21] M. Strenitzke, B. Derby, R.J. Brook, Alumina/silicon carbide nanocomposites by hybrid polymer/powder processing: microstructure and mechanical properties, J. Am. Ceram. Soc. 81 (1998) 41–48.
[22] S. Jiao, C.E. Borsa, C.N. Walker, The microstructures of alumina ceramics containing nanoparticles of silicon carbide or titanium nitride, Silic. Ind. 7–8 (1995) 211–214.
[23] S-M. Choi, T. Nishikawa, S. Honda, A role of the frontal process zone on toughening mechanism of polycrystalline ceramic materials and nanocomposites in: A.V. Duskin, X. Hu, E. Sahouryeh (Eds.), Structural Integrity and Fracture, Swets and Zeitlinger, Lisse 2002, pp. 383–388.
[24] T. Sekino, K. Niihara, Fabrication and mechanical properties of fine-tungsten-dispersed alumina-based composites, J. Mater. Sci. 32 (1997) 3943–3949.
[25] J. Selsing, Internal stresses in ceramics, J. Am. Ceram. Soc. 44 (1961) 419.
[26] H. Awaji, S-M. Choi, E. Yagi, Mechanisms of toughening and strengthening in ceramic-based nanocomposites, Mech. Mater. 34 (2002) 411–422.
[27] K.P.D. Lagerlöf, A.H. Heuer, J. Castaing, J.P. Rivière, T.E. Mitchell, Slip and twinning in sapphire α-(Al_2O_3), J. Am. Ceram. Soc. 77 (1994) 385–397.
[28] R.O. Ritchie, C.J. Gilbert, J.M. McNaney, Mechanics and mechanisms of fatigue damage and crack growth in advanced materials, Int. J. Solid Struct. 37 (2000) 311–329.
[29] H. Awaji, S-M. Choi, T. Ebisudani, D.D. Jayaseelan, J. Ceram. Soc. Jpn 108 (2000) 611–613 (in Japanese).
[30] R.G. Hoagland, J.D. Embury, A treatment of inelastic deformation around a crack tip due to microcracking, J. Am. Ceram. Soc. 63 (1980) 404–410.
[31] A.G. Evans, K.T. Faber, Toughening of ceramics by circumferential microcracking, J. Am. Ceram. Soc. 64 (1981) 394–398.
[32] H. Awaji, S-M. Choi, D.D. Jayaseelan, Indirect estimation of critical frontal process-zone size using a single-edge V-notched beam technique, J. Ceram. Soc. Jpn 109 (2001) 591–595.
[33] S-M. Choi, M. Okamoto, A novel technique for estimation of critical frontal process zone size in ceramics, Proceedings of the ASME Turbo Expo 2002, June 3–6, Amsterdam, 2002 pp. 1–5.
[34] H. Awaji, S-M. Choi, C.H. Chen, N. Kishi, J. Soc. Mater. Sci. Jpn 53 (2004) 1012–1018.
[35] H. Awaji, T. Watanabe, T. Yamada, Y. Sakaida, H. Tamiya, H. Nakagawa, Evaluation of fracture toughness by a single-edge V-notched beam method, Trans. Jpn Soc. Mech. Eng. 56A (1990) 1148–1153.
[36] H. Awaji, Y. Sakaida, V-notch technique for single-edge notched beam and chevron notch methods, J. Am. Ceram. Soc. 73 (1990) 3522–3523.
[37] M. Strandberg, Eng. Fract. Mech. 69 (2002) 403.
[38] C. H. Chen, H. Awaji, S-M. Choi, Critical frontal process zone size and fracture toughness, J. Ceram. Soc. Jpn. 112 (2004) S418–S422.
[39] S-M. Choi, S. Honda, T. Nishikawa, H. Awaji, T. Sekino, K. Niihara, Strengthening mechanism in alumina matrix nanocomposites, J. Soc. Mater. Sci. Jpn 52 (2003) 1374–1378.